Published in final edited form as:
Biomaterials. 2015 January ; 39: 39–46. doi:10.1016/j.biomaterials.2014.10.061.

VEGFR Targeting Leads to Significantly Enhanced Tumor Uptake of Nanographene Oxide in Vivo

Sixiang Shi[1], **Kai Yang**[2], **Hao Hong**[3], **Feng Chen**[3], **Hector F. Valdovinos**[4], **Shreya Goel**[1], **Todd E. Barnhart**[4], **Zhuang Liu**[2], and **Weibo Cai**[1,3,4,5,*]

[1]Materials Science Program, University of Wisconsin - Madison, WI, USA

[2]Jiangsu Key Laboratory for Carbon-Based Functional Materials and Devices, Institute of Functional Nano and Soft Materials Laboratory (FUNSOM), Soochow University, Suzhou, Jiangsu, China

[3]Department of Radiology, University of Wisconsin - Madison, WI, USA

[4]Department of Medical Physics, University of Wisconsin - Madison, WI, USA

[5]University of Wisconsin Carbone Cancer Center, Madison, WI, USA

Abstract

Although graphene oxide (GO) has recently been considered as a highly attractive nanomaterial for future cancer imaging and therapy, it is still a major challenge to improve its in vivo tumor active targeting efficiency. Here in this full article, we demonstrated the successful and significantly enhanced in vivo tumor vasculature targeting efficacy of well-functionalized GO nanoconjugates by using vascular endothelial growth factor 121 (VEGF121) as the targeting ligand. As-developed GO nanoconjugate exhibits excellent in vivo stability, specific in vitro and in vivo vascular endothelial growth factor receptor (VEGFR) targeting, significantly enhanced tumor accumulation (>8 %ID/g) as well as high tumor-to-muscle contrast, showing great potential for future tumor targeted imaging and therapy.

Keywords

graphene oxide (GO); vasculature targeting; positron emission tomography (PET); VEGF

1. Introduction

Graphene is a well-known material with single-layered carbon atoms packed into a two-dimensional honeycomb lattice [1]. Due to its unique mechanical, electronic, optical, and chemical properties, graphene has attracted tremendous interest over the last several years [2-6]. Among many different subtypes of graphene-based nanomaterials, graphene oxide (GO) with extremely high specific surface area has been recently accepted as an excellent platform for applications in biosensor, drug delivery, gene transfection, to name a few [7-12]. In addition, owing to the intrinsic high near-infrared (NIR) absorbance,

Corresponding Author: Weibo Cai, PhD, Departments of Radiology and Medical Physics, University of Wisconsin - Madison, Room 7137, 1111 Highland Ave, Madison, WI 53705-2275, USA., wcai@uwhealth.org; Phone: 608-262-1749; Fax: 608- 265-0614.

functionalized GO has also been employed for photothermal therapy in small animals [13-15].

However, challenges still exist. Most of current studies are focusing on in vivo passive targeted delivery of GO nanoconjugates with only limited tumor accumulation [16, 17]. Developing suitable in vivo active targeting strategies for further improving their targeting efficacy is still one of the major challenges in this field.

It is well accepted that tumor angiogenesis occurs when the tumor reaches a certain size (usually 1-2 mm in diameter), as new blood vessel formation is needed to supply oxygen and nutrients to cancer cells and to remove waste [18]. Tumor angiogenesis targeting (or vasculature targeting) has recently been accepted as a generally applicable in vivo targeting strategy for most of nanoparticles regardless of tumor types [19]. Vascular endothelial growth factor receptor (VEGFR) is a universal target overexpressed on vasculature of multiple solid tumor types and other disease models [20-22]. Being the naturally existing VEGFR ligand, $VEGF_{121}$ offers several advantages over the synthetic small-molecule VEGFR ligands or anti-VEGFR antibodies, and has much higher binding affinity to VEGFR (nanomolar range) than reported peptidic VEGFR inhibitors (submicromolar to micromolar range) [23].

Although $VEGF_{121}$ could serve as a promising targeting ligand for cancer diagnosis and treatment in preclinical studies and clinical trials, to date, few examples of positron emission tomography (PET) imaging with $VEGF_{121}$-conjugated nanoparticle have been reported [24]. Here, we aim for design and synthesis of a new type of GO-based tumor vasculature targeting nanoconjugate by surface engineering of GO with positron emission radioisotopes and $VEGF_{121}$, forming a novel GO nanoconjugate for non-invasive, quantitative and in vivo vasculature targeted tumor imaging.

2. Materials and methods

2.1. Reagents

$VEGF_{121}$ was provided by GenScript Corp. (Piscataway, NJ). S-2-(4-isothiocyanatobenzyl)-1,4,7-triazacyclononane-1,4,7-triacetic acid (p-SCN-Bn-NOTA) was purchased from Macrocyclics, Inc. (Dallas, TX). Chelex 100 resin (50-100 mesh) and fluoresce in isothiocyanate (FITC) were purchased from Sigma-Aldrich (St. Louis, MO). Succinimidyl carboxymethyl PEG maleimide (SCM-PEG-Mal; molecular weight: 5 kDa; Creative PEGworks, Winston Salem, NC), rat anti-mouse CD31 primary antibody (BD Biosciences, San Diego, CA), AlexaFluor488- or Cy3-labeled secondary antibodies (Jackson Immunoresearch Laboratories, Inc., West Grove, CA), Bevacizumab (Avastin, Genentech, San Francisco, CA) and PD-10 desalting columns (GE Healthcare, Piscataway, NJ) were all acquired from commercial sources. Water and all buffers were of Millipore grade and pre-treated with Chelex 100 resin to ensure that the aqueous solution was free of heavy metal. All other reaction buffers and chemicals were obtained from Thermo Fisher Scientific (Fair Lawn, NJ).

2.2. Synthesis of GO-PEG-NH_2

GO-PEG-NH_2 was synthesized by a similar process as detailed in our previous report [25, 26]. Briefly, GO was produced by a modified Hummers method, using flake expandable graphite as the original material. The prepared GO was mixed with 6-arm-polyethylene glycol-amine (10 kDa) at a weight ratio of 1:6 and reacted for ∼ 12 h in the presence of N-(3-dimethylaminopropyl-N'-ethylcarbodiimide) hydrochloride to form GO-PEG-NH_2. Excess PEG in the as-synthesized GO-PEG-NH_2 solution was removed by centrifuge filtration through 100 kDa MWCO Amicon filters and washed with water for 6 times. Atomic force microscopy and dynamic light scattering were performed to characterize the GO morphology and size distribution of nanoconjugates [27].

2.3. Synthesis of $VEGF_{121}$-SH

$VEGF_{121}$ was incubated with Traut's reagent at a molar ratio of 1:15 at pH 8.0 for 2 h. The resulting $VEGF_{121}$-SH was purified by size exclusion column chromatography with phosphate-buffered saline (PBS, pre-treated with Chelex 100 resin to prevent oxidation of the thiol) as the mobile phase.

2.4. Syntheses of GO-$VEGF_{121}$ nanoconjugates

GO-PEG-NH_2 was first mixed with p-SCN-Bn-NOTA at a molar ratio of 1:10 at pH 9.0, and reacted for 2 h at room temperature. The resulting NOTA-GO was purified by centrifugation with 100 kDa MWCO Amicon filters at 8,000 rpm for 15 min. Subsequently, NOTA-GO was reacted with SCM-PEG-Mal at a molar ratio of 1:30 at pH 8.5 for 2 h. The resulting NOTA-GOPEG-Mal was purified by centrifugation with 100 kDa MWCO Amicon filters at 8,000 rpm for 15min. Afterwards, NOTA-GO-PEG-Mal was reacted with $VEGF_{121}$-SH at a molar of 1:10 at pH 7.5 in the presence of tris(2-carboxyethyl)phosphine (TCEP). The final products were purified by size exclusion column chromatography and termed as NOTA-GO-$VEGF_{121}$. Similar strategies were used for the synthesis of FITC-GO-$VEGF_{121}$ and FITC-GO nanoconjugates.

2.5. Cell lines and animal model

4T1 murine breast cancer, U87MG human glioblastoma, and human umbilical vein endothelial cells (HUVECs) were obtained from the American Type Culture Collection (ATCC, Manassas, VA) and cultured as previously described [28]. Cells were used for in vitro and in vivo experiments when they reached ∼80 % confluence. All animal studies were conducted under a protocol approved by the University of Wisconsin Institutional Animal Care and Use Committee. Four- to five-week-old female nude mice (Harlan, Indianapolis, IN) were each injected with 2×10^6 U87MG cells in the flank to generate the U87MG glioblastoma model. The mice were used for in vivo experiments when the tumor diameter reached 4-6 mm.

2.6. Flow cytometry

HUVECs (VEGFR positive) [29] and 4T1 (VEGFR negative) [30] cells were harvested and suspended in cold PBS with 2 % bovine serum albumin at a concentration of 5×10^6 cells/mL. Cells were incubated with FITC-GO-$VEGF_{121}$ or FITC-GO at a concentration of

5 μg/mL (based on GO) for 30 min at room temperature before washing for three times with cold PBS. Subsequently, the cells were analyzed using a BD FACSCalibur 4-color analysis cytometer equipped with 488 nm and 633 nm lasers (Becton-Dickinson, San Jose, CA) and FlowJo analysis software (Tree Star, Inc., Ashland, OR).

2.7. ^{64}Cu labeling

^{64}Cu was produced with an onsite cyclotron (GE PETrace) in University of Wisconsin - Madison. $^{64}CuCl_2$ (74 MBq) was diluted in 300 μL of 0.1 M sodium acetate buffer (pH 6.5) and mixed with 50 μg of NOTA-GO-$VEGF_{121}$ or NOTA-GO. The reaction was conducted at 37 °C for 30 min with constant shaking [31, 32]. The resulting ^{64}Cu-NOTA-GO-$VEGF_{121}$ or ^{64}Cu-NOTA-GO was purified by size exclusion column chromatography using PBS as the mobile phase. The radioactive fractions containing ^{64}Cu-NOTA-GO-$VEGF_{121}$ or ^{64}Cu-NOTA-GO were collected for further in vitro and in vivo studies. Since all the GO nanoconjugates will contain the same NOTA and PEG chains, both “NOTA” and “PEG” were omitted from the acronyms of the final nanoconjugates for clarity.

2.8. Serum stability study

Serum stability study was carried out to ensure ^{64}Cu is stable on NOTA-GO-$VEGF_{121}$ for in vivo PET imaging. ^{64}Cu-NOTA-GO-$VEGF_{121}$ was incubated in PBS and complete serum at 37 °C for up to 48 h. At different time points, portions of the mixture were sampled and filtered through 100 kDa MWCO filters. The radioactivity that remained on the filter was measured after discarding the filtrate. The retained (i.e., intact) ^{64}Cu on NOTA-GO-$VEGF_{121}$ was calculated using the equation (radioactivity on filter/total sampled radioactivity × 100%).

2.9. In vivo VEGFR targeted PET imaging and biodistribution studies

U87MG tumor-bearing mice were each intravenously injected with 5-10 MBq of ^{64}Cu-NOTA-GO-$VEGF_{121}$ or ^{64}Cu-NOTA-GO via tail vein. Serial PET scans were performed at various time points post-injection (p.i.) with using a micro PET/micro CT Inveon rodent model scanner (Siemens Medical Solutions USA, Inc.). Data acquisition, image re-construction, and ROI analysis of the PET data were performed as described previously [26, 31]. Quantitative PET data of the U87MG tumor and major organs was presented as %ID/g. After the last scan at 48 h p.i., biodistribution studies were carried out to confirm that the %ID/g values based on PET imaging truly represented the radioactivity distribution in mice. Mice were euthanized and U87MG tumor, blood and major organs/tissues were collected and wet-weighed. The radioactivity in the tissue was measured using a γ counter (PerkinElmer) and presented as %ID/g (mean ± SD).

2.10. Histology

U87MG tumor-bearing mice were intravenously injected with GO-$VEGF_{121}$ and GO (5 mg/kg of mouse body weight) and euthanized at 3 h p.i. (when U87MG tumor uptake was at the peak based on PET imaging). Organs including U87MG tumor, liver, spleen and muscle were frozen and cryo-sectioned for histological analysis. Frozen tissue slices of 7 μm thickness were fixed with cold acetone and stained for endothelial marker CD31 by using a

rat anti-mouse CD31 antibody and a Cy3-labeled donkey anti-rat IgG [33]. To stain $VEGF_{121}$, the same tissue slices were also incubated with Avastin (primary antibody) [34] and then AlexaFluor488-labeled goat anti-human IgG (secondary antibody). All images were acquired by using a Nikon Eclipse Ti microscope.

3. Results and discussion

3.1. Synthesis and characterization of GO nanoconjugates

GO was produced by Hummers method and modified with six-armed branched polyethylene glycol (PEG) as previously reported for enhanced in vivo stability and biocompatibility [8, 25]. The presence of amine groups at the terminal end could facilitate the further covalent conjugation of various functional entities. PEGylated GO (i.e. GO-PEG-NH_2) was then functionalized with 1,4,7-triazacyclononane-1,4,7-triacetic acid (NOTA) (a well-known chelator for copper-64 (^{64}Cu, $t_{1/2}$=12.7 h) labeling) and $VEGF_{121}$ as the targeting ligand for in vivo vasculature targeting.

A schematic structure of final GO nanoconjugate (i.e. ^{64}Cu-NOTA-GO-PEG-$VEGF_{121}$) after surface engineering is shown in Figure 1A. As synthesized GO-PEG-NH_2 existed a size range of 20-50 nm (Figure 1b), based on atomic force microscopy (AFM) measurements (Figure 1B). Dynamic light scattering (DLS) study showed that GO-PEG-NH_2 has a hydrodynamic diameter of 27.7 ± 5.8 nm, whereas the diameter of NOTA-GO-$VEGF_{121}$ was found to be 32.9 ± 3.0 nm (Figure 1C). Since all the GO nanoconjugates will contain the same NOTA and PEG chains, in the following sections both “NOTA” and “PEG” were omitted from the acronyms of the final nanoconjugates for clarity.

3.2. In vitro VEGFR targeting

To validate in vitro VEGFR targeting capability of GO-$VEGF_{121}$ nanoconjugates, flow cytometry was carried out in human umbilical vein endothelial cells (HUVECs, VEGFR positive) [29] and 4T1 murine breast cancer cells (VEGFR negative) [30]. Fluoresce in isothiocyanate (FITC) was further conjugated to GO-$VEGF_{121}$ to form FITC-GO-$VEGF_{121}$ (targeted group). FITC-conjugated GO with no $VEGF_{121}$ (i.e. FITC-GO, non-targeted group) was used as the control. As evidenced in Figure 2A, the fluorescence signal from HUVECs was significantly enhanced (∼20 fold higher than the negative control group) upon incubation with FITC-GO-$VEGF_{121}$, whereas only slight fluorescence enhancement was observed upon FITC-GO treatment. Note, concentration of GO and in vitro incubation time were all kept the same. No significant fluorescence signal enhancement was observed when using 4T1 cell line for both targeted and non-targeted groups. Taken together, flow cytometry results clearly demonstrated high VEGFR targeting specificity and minimal non-specific binding of GO-$VEGF_{121}$ nanoconjugates.

3.3. In vivo VEGFR targeting and ex vivo biodistribution studies

Previously, we reported PET imaging of VEGFR expression level using ^{64}Cu-labeled $VEGF_{121}$, and demonstrated higher VEGFR expression in smaller (∼60 mm^3) U87MG glioblastoma tumors when compared with larger ones (∼1,200 mm^3) [35]. In current study,

U87MG tumor-bearing mice with tumor volume of ~60 mm^3 were used for in vivo targeted PET imaging studies.

Both GO-$VEGF_{121}$ and GO nanoconjugates were labeled with ^{64}Cu, and purified by PD-10 column, to form ^{64}Cu-GO-$VEGF_{121}$ and ^{64}Cu-GO, respectively. In vitro serum stability was later performed by incubating ^{64}Cu-GO-$VEGF_{121}$ with complete mouse serum at 37 °C for 48 h (Figure 2B). Our results showed that more than 95% of ^{64}Cu remained on the GO-$VEGF_{121}$ nanoconjugates, indicating high stability of ^{64}Cu-GO-$VEGF_{121}$ in mouse serum.

As prepared ^{64}Cu-GO-$VEGF_{121}$ and ^{64}Cu-GO were later intravenously injected to U87MG tumor-bearing mice and imaged using a micro PET/microCT Inveon rodent model scanner at 0.5, 3, 6, 16, 24 and 48 h post-injection (p.i.). Coronal PET images that contain the U87MG tumors are shown in Figure 3, and the quantitative data obtained from region-of-interest (ROI) analysis of the PET data are shown in Figure 4, Table S1 and Table S2.

Systematic PET imaging and quantification analysis showed that U87MG tumor uptake of ^{64}Cu-GO-$VEGF_{121}$ (i.e. targeted group) could be clearly visible at 0.5 h p.i. (6.5 ± 1.7 percentage injected dose per gram of tissue [%ID/g]) and peaked at 3 h p.i. with tumor accumulation found to be 8.2 ± 1.4 %ID/g (Figure 3A, 4A, Table S1). While, without the conjugation of $VEGF_{121}$, the accumulation of ^{64}Cu-GO was found ~2 fold lower at all time points examined (Figure 3B, 4B,C, Table S2), clearly indicating that conjugation of $VEGF_{121}$ to GO could increase tumor uptake through active targeting of VEGFR on the tumor vasculature. Beside higher tumor accumulation, tumor-to-muscle (T/M) ratio was improved as well. The highest T/M ratio in targeted group was found to be 8.4 ± 2.1, which is >2 fold higher than the non-targeted group (Figure 4D, Table S3).

Similar as what we observed in other GO nanoconjugates [26, 31, 36], besides tumor uptake, most of ^{64}Cu-GO-$VEGF_{121}$ was found in liver with the highest uptake estimated to be 24.9 ± 3.0 %ID/g at 0.5 h p.i. and gradually decreased to 10.1 ± 0.5 %ID/g at 48 h p.i. (n=4, Figure 3A, 4A, Table S1). Similar high liver uptake was also observed in the non-targeted group (n=4, Figure 3B, 4B, Table S2).

To further confirm the accuracy of PET quantification analysis, ex vivo biodistribution studies were carried out at 3 h p.i. (when tumor uptake peaked based on PET imaging in Figure 3A) and 48 h p.i. (after the last PET scan). As shown in Figure 5, the quantitative results based on PET and biodistribution studies matched very well, confirming that serial non-invasive PET imaging accurately reflected the distribution of ^{64}Cu-GO-$VEGF_{121}$ and ^{64}Cu-GO in U87MG tumor-bearing mice.

3.4. Histology

To further confirm that tumor uptake of ^{64}Cu-GO-$VEGF_{121}$ is VEGFR specific and GO nanoconjugates were indeed delivered to the tumor, histological studies were performed. U87MG tumor-bearing mice were intravenously injected with GO-$VEGF_{121}$ and GO (dose: 5 mg/kg) and euthanized at 3 h p.i. (when U87MG tumor uptake was at the peak based on PET imaging). Organs including U87MG tumor, liver, spleen and muscle were collected,

frozen and cryo-sectioned for histological analysis. Well-established protocols were later used for the staining of CD31 and $VEGF_{121}$ [33, 34].

As shown in Figure 6A, GO-$VEGF_{121}$ distribution in the U87MG tumor was found primary on the vasculature with little extravasation, as evidenced by the excellent overlay of the CD31 (red) and GO-$VEGF_{121}$ (green), while no obvious green signal could be found in U87MG tumor from the non-targeted group (Figure 6B). Strong green fluorescence signal from the liver and spleen slices were observed outside the vasculature, indicating non-specific RES uptake and hepatobiliary clearance of GO-$VEGF_{121}$ (Figure 6C,D). In addition, little green fluorescence was observed in the muscle, which is consistent with the results of PET and biodistribution studies (Figure 6E). Taken together, our histology study clearly demonstrated the VEGFR targeting specificity of GO-$VEGF_{121}$.

4. Conclusion

In conclusion, we reported the surface engineering and in vivo tumor vasculature targeting of GO nanoconjugates in U87MG tumor-bearing mice, with ^{64}Cu as the radiolabel and $VEGF_{121}$ as the targeting ligand. Excellent stability and high targeting specificity of GO-$VEGF_{121}$ were achieved based on systematic in vivo/in vitro/ex vivo studies. More importantly, our newly developed ^{64}Cu-GO-$VEGF_{121}$ nanoconjugate was able to target vascular VEGFR efficiently in U87MG model with the highest tumor uptake found to be >8 %ID/g, giving an extra boost to tumor uptake based on passive targeting alone (∼4 %ID/g). We believe that GO-$VEGF_{121}$ with significantly improved tumor targeting efficiency could inspire future design of smart GO-based nanosystems and show great potential for enhanced theranostics in living systems.

Supplementary Material

Refer to Web version on PubMed Central for supplementary material.

Acknowledgments

This work is supported, in part, by the University of Wisconsin-Madison, the National Institutes of Health (NIBIB/NCI 1R01CA169365 and P30CA014520), the Department of Defense (W81XWH-11-1-0644), the American Cancer Society (125246-RSG-13-099-01-CCE), the National Basic Research Program of China (973 Program, 2012CB932601 & 2011CB911002), and the National Science Foundation of China (51002100 & 51222203).

References

1. Novoselov KS, Geim AK, Morozov SV, Jiang D, Zhang Y, Dubonos SV, et al. Electric field effect in atomically thin carbon films. Science. 2004; 306:666–9. [PubMed: 15499015]
2. Geim AK, Novoselov KS. The rise of graphene. Nat Mater. 2007; 6:183–91. [PubMed: 17330084]
3. Huang X, Yin Z, Wu S, Qi X, He Q, Zhang Q, et al. Graphene-based materials: synthesis, characterization, properties, and applications. Small. 2011; 7:1876–902. [PubMed: 21630440]
4. Pumera M. Graphene-based nanomaterials and their electrochemistry. Chem Soc Rev. 2010; 39:4146–57. [PubMed: 20623061]
5. Service RF. Materials science. Carbon sheets an atom thick give rise to graphene dreams. Science. 2009; 324:875–7. [PubMed: 19443761]

6. Li X, Wang X, Zhang L, Lee S, Dai H. Chemically derived, ultrasmooth graphene nanoribbon semiconductors. Science. 2008; 319:1229–32. [PubMed: 18218865]
7. Feng L, Zhang S, Liu Z. Graphene based gene transfection. Nanoscale. 2011; 3:1252–7. [PubMed: 21270989]
8. Liu Z, Robinson JT, Sun X, Dai H. PEGylated nanographene oxide for delivery of waterinsoluble cancer drugs. J Am Chem Soc. 2008; 130:10876–7. [PubMed: 18661992]
9. Tang LA, Wang J, Loh KP. Graphene-based SELDI probe with ultrahigh extraction and sensitivity for DNA oligomer. J Am Chem Soc. 2010; 132:10976–7. [PubMed: 20698647]
10. Zhou M, Zhang R, Huang M, Lu W, Song S, Melancon MP, et al. A chelator-free multifunctional [64Cu]CuS nanoparticle platform for simultaneous micro-PET/CT imaging and photothermal ablation therapy. J Am Chem Soc. 2010; 132:15351–8. [PubMed: 20942456]
11. Zhang L, Lu Z, Zhao Q, Huang J, Shen H, Zhang Z. Enhanced chemotherapy efficacy by sequential delivery of siRNA and anticancer drugs using PEI-grafted graphene oxide. Small. 2011; 7:460–4. [PubMed: 21360803]
12. He S, Song B, Li D, Zhu C, Qi W, Wen Y, et al. A Graphene Nanoprobe for Rapid, Sensitive, and Multicolor Fluorescent DNA Analysis. Adv Funct Mater. 2010; 20:453–9.
13. Yang K, Wan J, Zhang S, Tian B, Zhang Y, Liu Z. The influence of surface chemistry and size of nanoscale graphene oxide on photothermal therapy of cancer using ultra-low laser power. Biomaterials. 2012; 33:2206–14. [PubMed: 22169821]
14. Huang P, Xu C, Lin J, Wang C, Wang X, Zhang C, et al. Folic Acid-conjugated Graphene Oxide loaded with Photosensitizers for Targeting Photodynamic Therapy. Theranostics. 2011; 1:240–50. [PubMed: 21562631]
15. Zhou L, Wang W, Tang J, Zhou JH, Jiang HJ, Shen J. Graphene oxide noncovalent photosensitizer and its anticancer activity in vitro. Chemistry. 2011; 17:12084–91. [PubMed: 21915922]
16. Yang K, Hu LL, Ma XX, Ye SQ, Cheng L, Shi XZ, et al. Multimodal Imaging Guided Photothermal Therapy using Functionalized Graphene Nanosheets Anchored with Magnetic Nanoparticles. Adv Mater. 2012; 24:1868–72. [PubMed: 22378564]
17. Miao W, Shim G, Lee S, Choe YS, Oh YK. Safety and tumor tissue accumulation of pegylated graphene oxide nanosheets for co-delivery of anticancer drug and photosensitizer. Biomaterials. 2013; 34:3402–10. [PubMed: 23380350]
18. Folkman J. Tumor angiogenesis: therapeutic implications. New Engl J Med. 1971; 285:1182–6. [PubMed: 4938153]
19. Chen F, Cai W. Tumor vasculature targeting: a generally applicable approach for functionalized nanomaterials. Small. 2014; 10:1887–93. [PubMed: 24591109]
20. Ferrara N. The role of VEGF in the regulation of physiological and pathological angiogenesis. EXS. 2005:209–31. [PubMed: 15617481]
21. Chen F, Zhang Y, Cai W. Molecular MRI of VEGFR-2 reveals intra-tumor and inter-tumor heterogeneity. Am J Nucl Med Mol Imaging. 2013; 3:312–6. [PubMed: 23900733]
22. Sun ZC, Huang P, Tong G, Lin J, Jin A, Rong PF, et al. VEGF-loaded graphene oxide as theranostics for multi-modality imaging-monitored targeting therapeutic angiogenesis of ischemic muscle. Nanoscale. 2013; 5:6857–66. [PubMed: 23770832]
23. El-Mousawi M, Tchistiakova L, Yurchenko L, Pietrzynski G, Moreno M, Stanimirovic D, et al. A vascular endothelial growth factor high affinity receptor 1-specific peptide with antiangiogenic activity identified using a phage display peptide library. J Biol Chem. 2003; 278:46681–91. [PubMed: 12954624]
24. Chen K, Li ZB, Wang H, Cai W, Chen X. Dual-modality optical and positron emission tomography imaging of vascular endothelial growth factor receptor on tumor vasculature using quantum dots. Eur J Nucl Med Mol Imaging. 2008; 35:2235–44. [PubMed: 18566815]
25. Yang K, Zhang S, Zhang G, Sun X, Lee ST, Liu Z. Graphene in mice: ultrahigh in vivo tumor uptake and efficient photothermal therapy. Nano Lett. 2010; 10:3318–23. [PubMed: 20684528]
26. Hong H, Yang K, Zhang Y, Engle JW, Feng L, Yang Y, et al. In vivo targeting and imaging of tumor vasculature with radiolabeled, antibody-conjugated nanographene. ACS Nano. 2012; 6:2361–70. [PubMed: 22339280]

27. Yang K, Feng L, Hong H, Cai W, Liu Z. Preparation and functionalization of graphene nanocomposites for biomedical applications. Nat Protoc. 2013; 8:2392–403. [PubMed: 24202553]
28. Hong H, Zhang Y, Severin GW, Yang Y, Engle JW, Niu G, et al. Multimodality Imaging of Breast Cancer Experimental Lung Metastasis with Bioluminescence and a Monoclonal Antibody Dual-Labeled with (89)Zr and IRDye 800CW. Mol Pharm. 2012; 9:2339–49. [PubMed: 22784250]
29. Imoukhuede PI, Popel AS. Expression of VEGF receptors on endothelial cells in mouse skeletal muscle. PLoS One. 2012; 7:e44791. [PubMed: 22984559]
30. Willmann JK, Lutz AM, Paulmurugan R, Patel MR, Chu P, Rosenberg J, et al. Dualtargeted contrast agent for US assessment of tumor angiogenesis in vivo. Radiology. 2008; 248:936–44. [PubMed: 18710985]
31. Shi S, Yang K, Hong H, Valdovinos HF, Nayak TR, Zhang Y, et al. Tumor vasculature targeting and imaging in living mice with reduced graphene oxide. Biomaterials. 2013; 34:3002–9. [PubMed: 23374706]
32. Orbay H, Zhang Y, Valdovinos HF, Song G, Hernandez R, Theuer CP, et al. Positron emission tomography imaging of CD105 expression in a rat myocardial infarction model with (64)Cu-NOTA-TRC105. Am J Nucl Med Mol Imaging. 2013; 4:1–9. [PubMed: 24380040]
33. Hong H, Yang Y, Zhang Y, Engle JW, Barnhart TE, Nickles RJ, et al. Positron emission tomography imaging of CD105 expression during tumor angiogenesis. Eur J Nucl Med Mol Imaging. 2011; 38:1335–43. [PubMed: 21373764]
34. Lambrechts D, Lenz HJ, de Haas S, Carmeliet P, Scherer SJ. Markers of response for the antiangiogenic agent bevacizumab. J Clin Oncol. 2013; 31:1219–30. [PubMed: 23401453]
35. Cai W, Chen K, Mohamedali KA, Cao Q, Gambhir SS, Rosenblum MG, et al. PET of vascular endothelial growth factor receptor expression. J Nucl Med. 2006; 47:2048–56. [PubMed: 17138749]
36. Hong H, Zhang Y, Engle JW, Nayak TR, Theuer CP, Nickles RJ, et al. In vivo targeting and positron emission tomography imaging of tumor vasculature with (66)Ga-labeled nano-graphene. Biomaterials. 2012; 33:4147–56. [PubMed: 22386918]

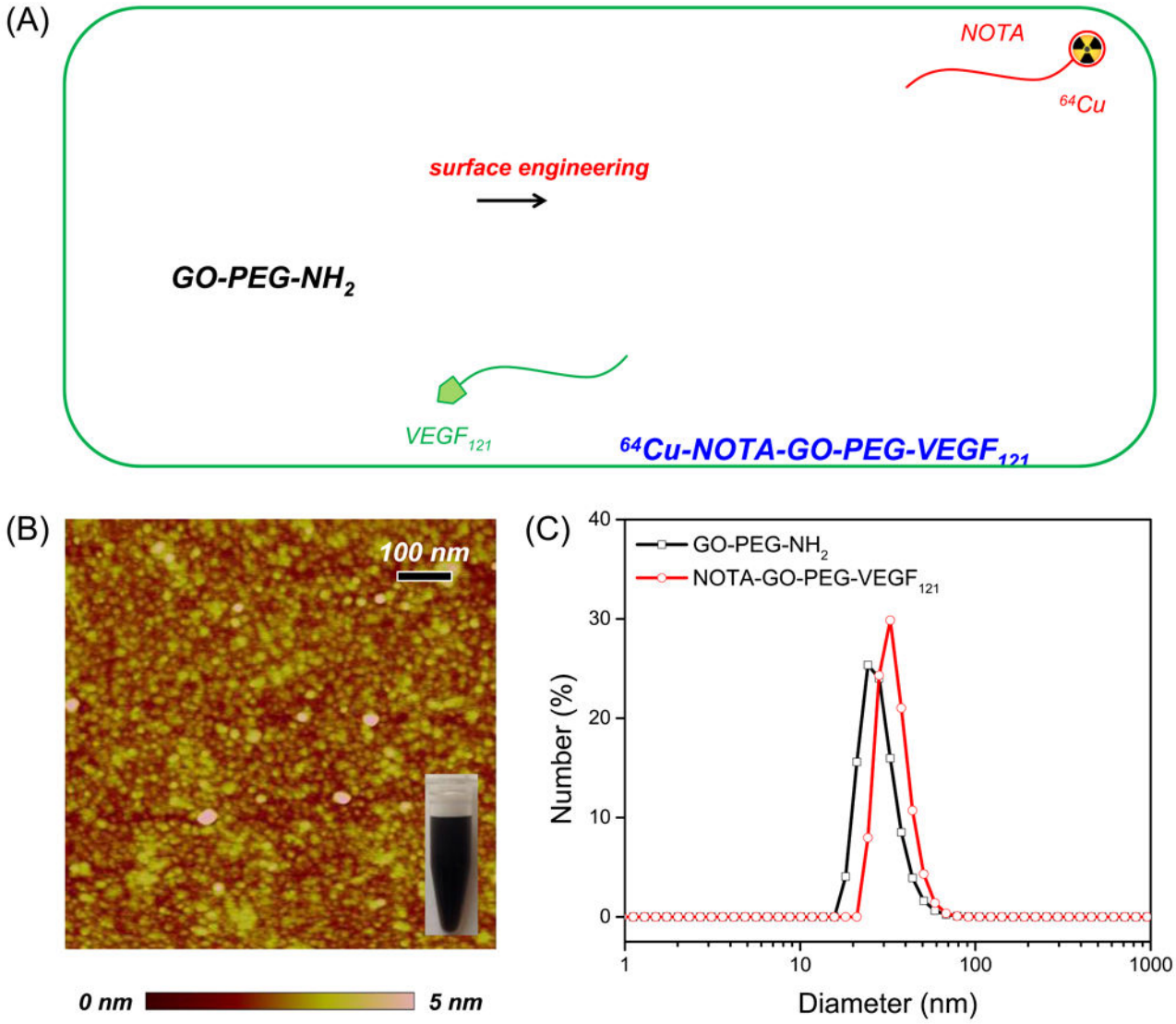

Figure 1.

(**A**) A schematic illustration showing the surface engineering of GO nanoconjugates. (**B**) AFM image of GO-PEG-NH_2. (**C**) DLS size distribution of the GO-PEG-NH_2 (black line) and NOTA-GO-PEG-$VEGF_{121}$ nanoconjugates (red line).

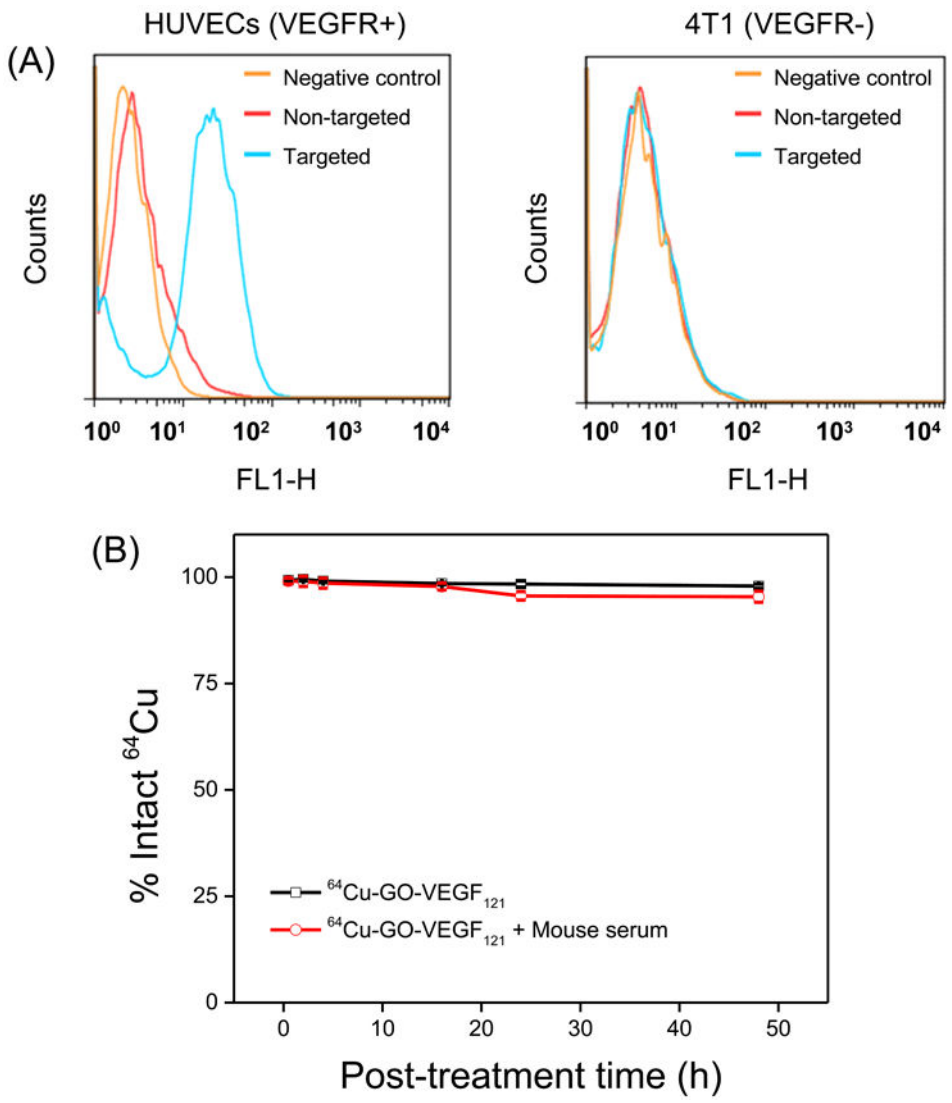

Figure 2.

In vitro VEGFR targeting and serum stability studies. (**A**) Flow cytometry analysis of the GO nanoconjugates in HUVECs (VEGFR+) and 4T1 breast cancer cells (VEGFR-). (**B**) Serum stability study of ^{64}Cu-GO-VEGF$_{121}$ at 37 °C for 48 h.

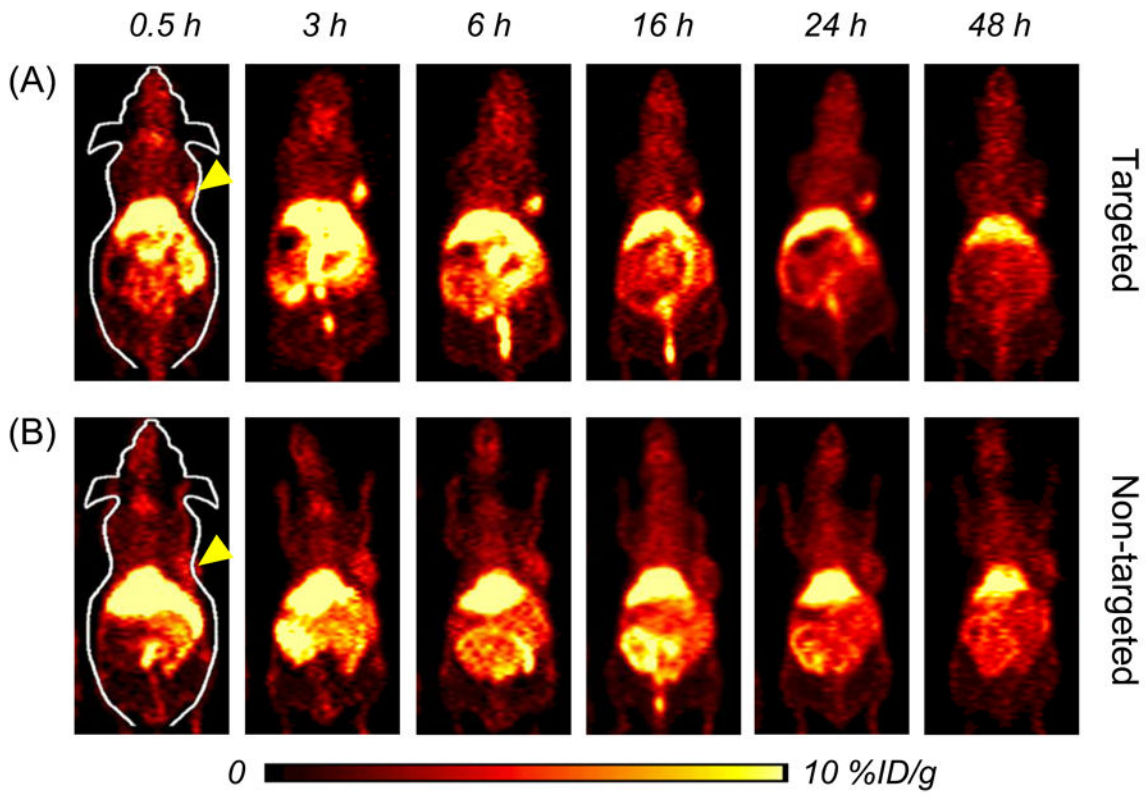

Figure 3.

In vivo VEGFR targeted PET imaging. Serial coronal PET images of U87MG tumor bearing mice at different time points post-injection of (**A**) ^{64}Cu-GO-VEGF$_{121}$ (targeted group) and (**B**) ^{64}Cu-GO (non-targeted group). Tumors are indicated by yellow arrowheads.

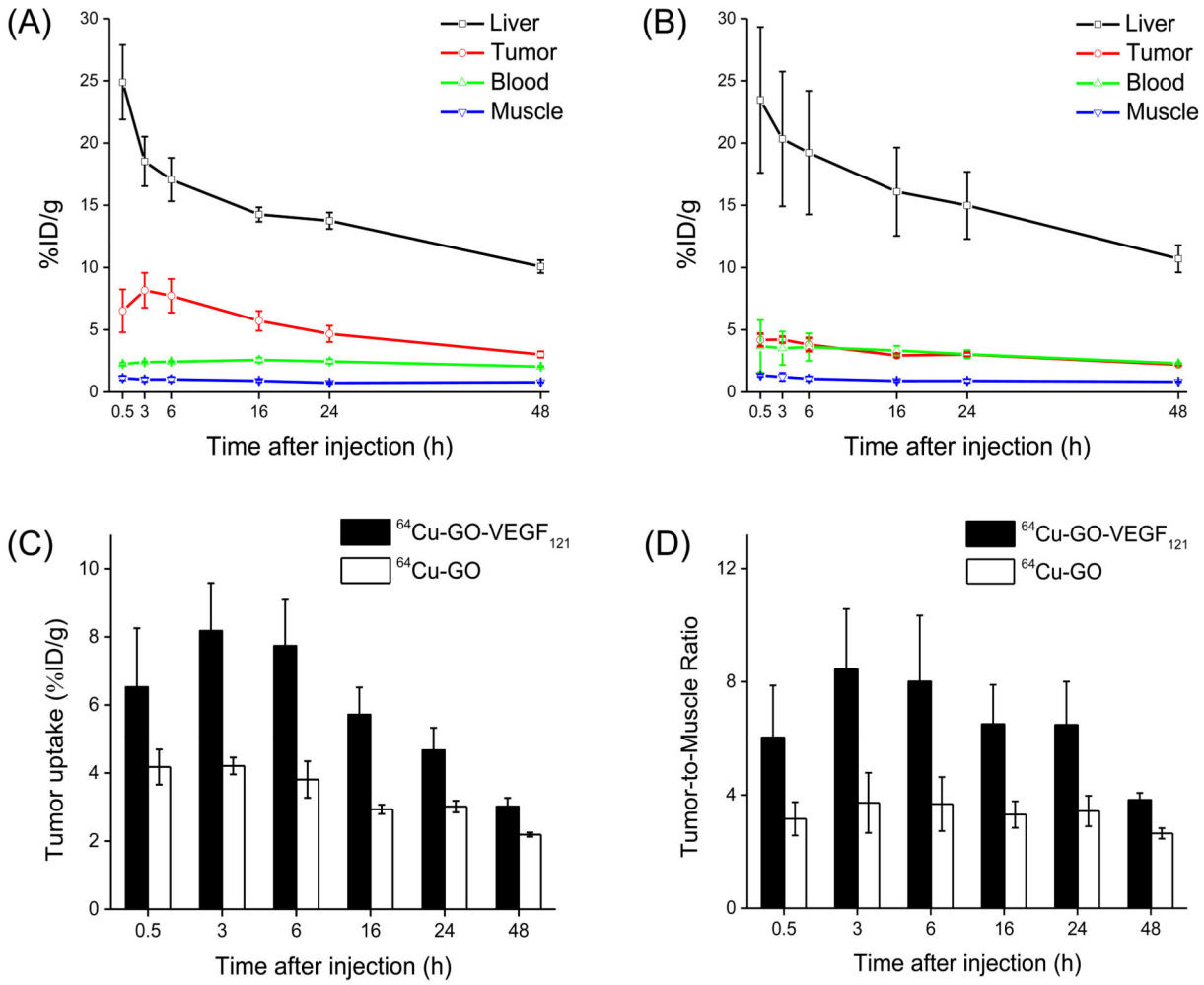

Figure 4.

Quantitative analysis of the PET data. (**A**) Time activity curves of the liver, U87MG tumor, blood, and muscle upon intravenous injection of ^{64}Cu-GO-VEGF$_{121}$ (targeted group). (**B**) Time activity curves of the liver, U87MG tumor, blood, and muscle upon intravenous injection of ^{64}Cu-GO (non-targeted group). (**C**) Comparison of the U87MG tumor uptake in both targeted and non-targeted groups. (**D**) Comparison of the tumor-to-muscle ratio in targeted and non-targeted groups. The differences between the tumor uptake and tumor-to-muscle ratio of ^{64}Cu-GO-VEGF$_{121}$ and ^{64}Cu-GO were statistically significant ($P < 0.05$) at all time points. All data represent 4 mice per group.

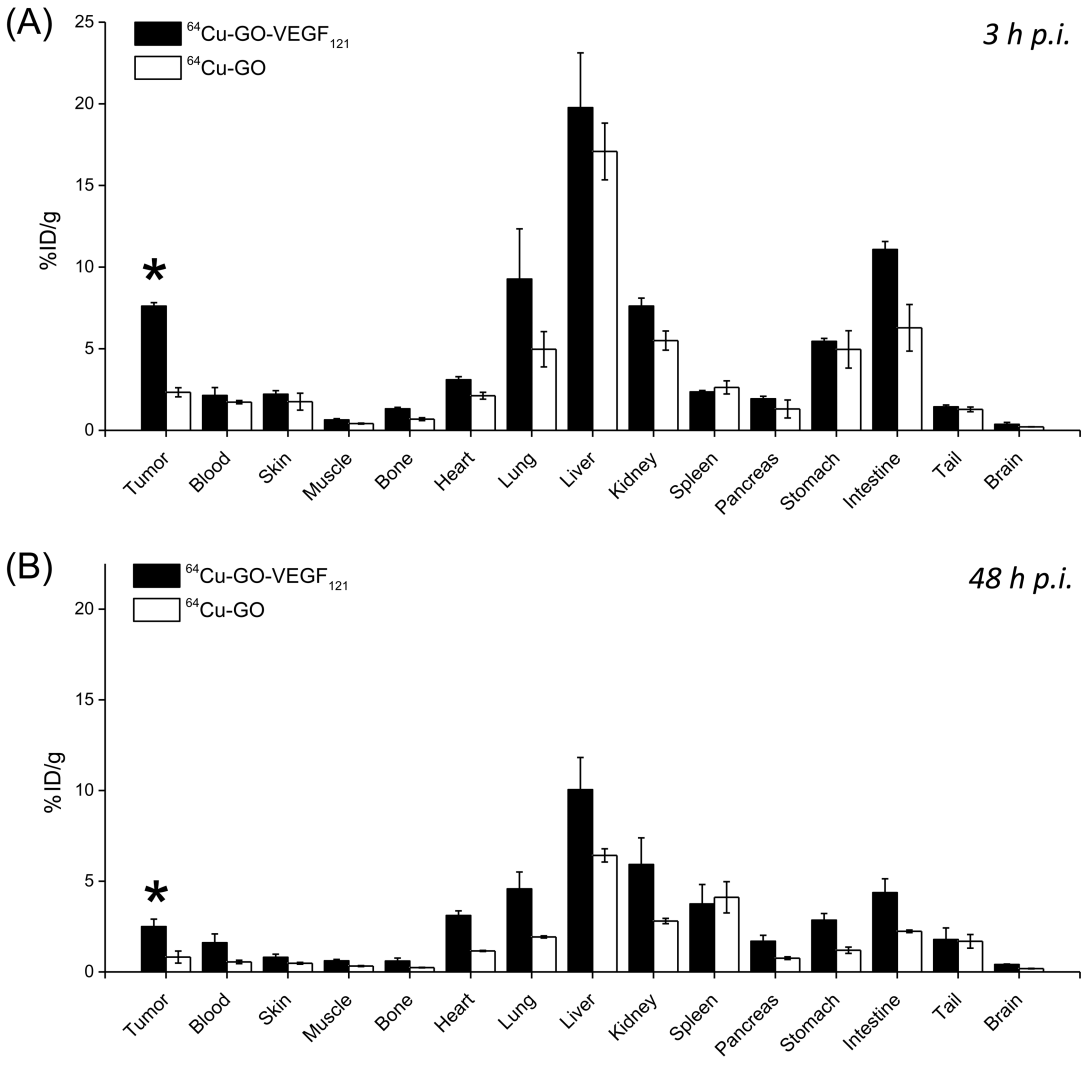

Figure 5.

Biodistribution studies in U87MG tumor-bearing mice at (**A**) 3 h and (**B**) 48 h post-injection of the GO nanoconjugates. All data represent 4 mice per group.

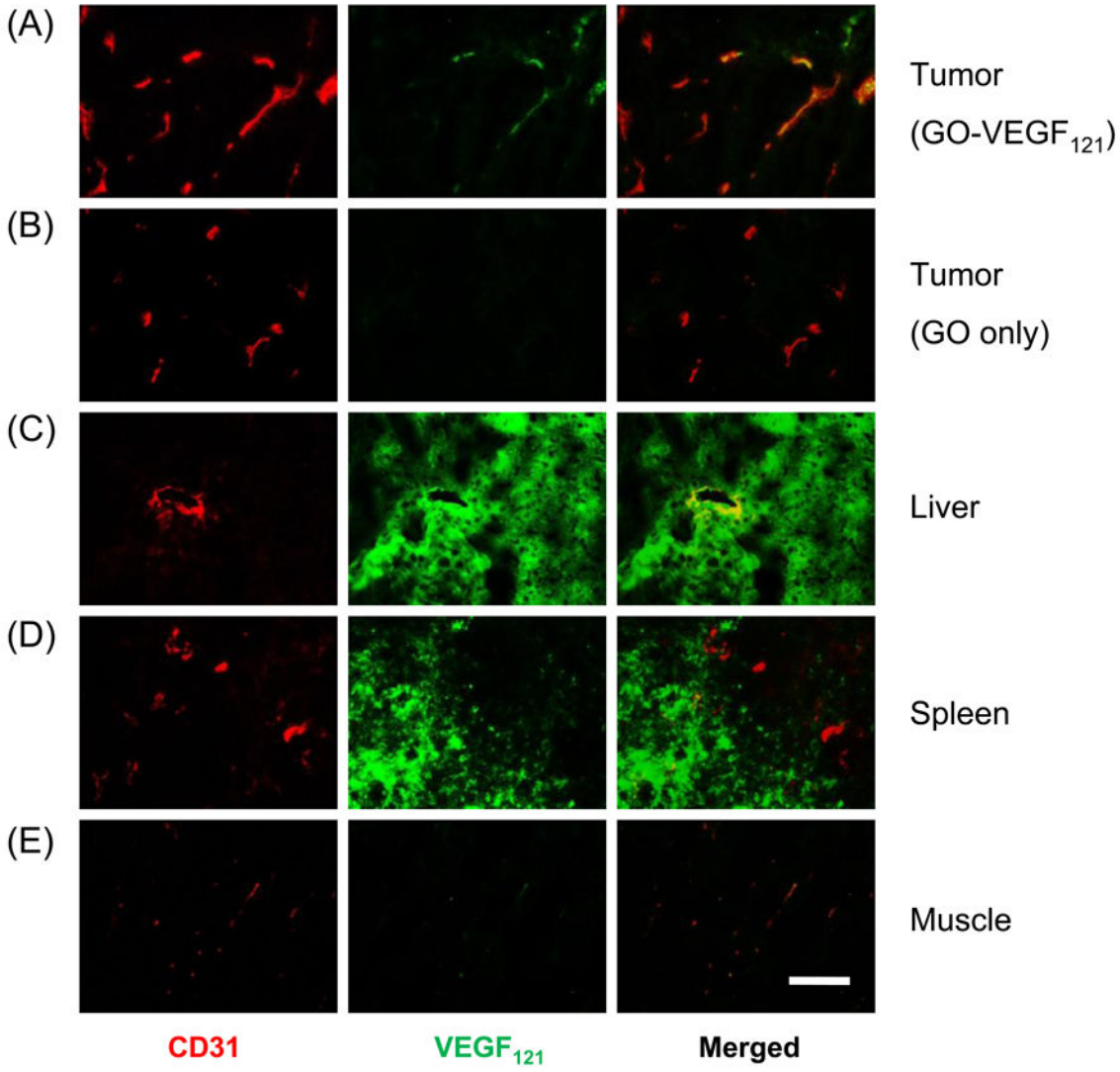

Figure 6.

Histology study. Immunofluorescence staining of various tissue slices of (**A**) U87MG tumor (targeted group), (**B**) U87MG tumor (non-targeted group), (**C**) Liver, (**D**) Spleen and (**E**) Muscle. Red staining represents CD31 (using anti-mouse CD31 primary antibody), while green staining represents GO-$VEGF_{121}$ (using Avastin as the primary antibody). Scale bar: 100 μm. Note, Slices of liver, spleen and muscle were all from targeted group.